DESY 20-216, MS-TP-20-44, LTH 1248

arXiv:2012.10298v1 [hep-ph] 18 Dec 2020

Longitudinal Z-Boson Polarization and the Higgs Boson Production Cross Section at the Large Hadron Collider

S. Amoroso,[1,*] J. Fiaschi,[2,3,†] F. Giuli,[4,5,‡] A. Glazov,[1,§] F. Hautmann,[6,7,¶] and O. Zenaiev[4,**]

[1] *Deutsches Elektronen-Synchrotron DESY, D 22607 Hamburg*
[2] *Department of Mathematical Sciences, University of Liverpool, Liverpool L69 3BX*
[3] *Institut für Theoretische Physik, Universität Münster, D 48149 Münster*
[4] *CERN, CH-1211 Geneva 23, Switzerland*
[5] *University of Rome Tor Vergata and INFN, Sezione di Roma 2, 00133 Roma*
[6] *Elementaire Deeltjes Fysica, Universiteit Antwerpen, B 2020 Antwerpen*
[7] *Theoretical Physics Department, University of Oxford, Oxford OX1 3PU*

Lepton pairs are produced copiously in high-energy hadron collisions via electroweak gauge boson exchange, and are one of the most precisely measured final states in proton-proton collisions at the Large Hadron Collider (LHC). We propose that measurements of lepton angular distributions can be used to improve the accuracy of theoretical predictions for Higgs boson production cross sections at the LHC. To this end, we exploit the sensitivity of the lepton angular coefficient associated with the longitudinal Z-boson polarization to the parton density function (PDF) for gluons resolved from the incoming protons, in order to constrain the Higgs boson cross section from gluon fusion processes. By a detailed numerical analysis using the open-source platform `xFitter`, we find that high-statistics determinations of the longitudinally polarized angular coefficient at the LHC Run III and high-luminosity HL-LHC improve the PDF systematics of the Higgs boson cross section predictions by 50 % over a broad range of Higgs boson rapidities.

Introduction. Precision studies in the Higgs sector of the Standard Model (SM) are central to current [1] and forthcoming [2] physics programs at the Large Hadron Collider (LHC), and provide a portal to searches for beyond-Standard-Model (BSM) physics. The dominant mechanism for the production of Higgs bosons in proton-proton collisions at the LHC is given by the fusion of two gluons resolved from the incoming protons. With the very high accuracy reached in perturbative Quantum Chromodynamics (QCD) calculations of gluon-initiated production cross sections, currently of next-to-next-to-next-to-leading order (N^{3}LO) [3, 4] in the QCD coupling α_s, the theoretical systematics affecting the predictions for gluon fusion processes receives essential contributions from the non-perturbative gluon parton density function (PDF), as well as the sea-quark densities coupled to gluons through the initial-state QCD evolution.

The primary source of knowledge of the gluon PDF is given at present, in global fits to hadron collider data [5–11], by deep inelastic scattering (DIS) experimental measurements at high energy. Future DIS experiments [12, 13] are proposed to extend the range and accuracy of our current knowledge of the gluon PDF. It is hoped that substantial progress can also come from measurements at the LHC itself, particularly in the forthcoming high-luminosity phase HL-LHC [14]. Gluon PDF determinations are considered from open [15, 16] and bound-state [17] charm and bottom quark production, light-quark jets [18] and top quark production [19].

In this work we take color-singlet hadro-production (unlike the above cases, in which the Born-approximation final state contains colored particles) and, similarly to the case of DIS, investigate the sensitivity to the gluon PDF via $\mathcal{O}(\alpha_s)$ contributions, guided by criteria of perturbative stability and experimental precision.

Consider Drell-Yan (DY) lepton-pair production [20] via electroweak vector boson exchange. Let us map the DY cross section in the boson invariant mass M, rapidity Y and transverse momentum p_T, and in the lepton polar and azimuthal angles θ and ϕ, defined in the Collins-Soper reference frame [21]. The DY cross section summed over the electroweak boson polarizations has the angular distribution $1 + \cos^2\theta$ and is sensitive to the gluon PDF for finite p_T. However, in the p_T region where the cross section is largest, it is affected by large perturbative corrections to all orders in α_s (see e.g. [22], and references therein). Let us turn to contributions of the single electroweak-boson polarizations. The diagonal elements of the polarization density matrix in the helicity basis yield (besides the unpolarized cross section, proportional to the trace of the density matrix) the forward-backward asymmetry and the longitudinally polarized cross section [21, 23–25], associated respectively with angular distributions $\cos\theta$ and $(3\cos^2\theta - 1)/2$. The former is parity-violating and dominated by flavor non-singlet PDFs [26–32]. The latter is parity-conserving and sensitive to flavor singlet PDFs. Off-diagonal density matrix elements can be accessed by measuring, besides θ, the lepton's azimuthal angle ϕ, and yield six additional contributions besides the previous three, leading to nine linearly independent polarized cross sections, which correspond to the nine terms in the expansion over spherical harmonics $Y_j^m(\theta,\phi)$ with $j \leq 2$.

In order to constrain the Higgs boson production cross section from gluon fusion, we will focus on the ratio of the longitudinal electroweak boson cross section to the unpolarized cross section, defining the angular coefficient

$$A_0(s, M, Y, p_T) = \frac{2d\sigma^{(L)}/dMdYdp_T}{d\sigma/dMdYdp_T}. \qquad (1)$$

The coefficient A_0 is perturbatively stable, as illustrated by the smallness of its next-to-leading-order (NLO) [33–38] and next-to-next-to-leading-order (NNLO) [39] radiative corrections for finite p_T, and precisely measured at the LHC [40, 41], following earlier measurements at the Tevatron [42] and fixed-target experiments [43–47]. We will comment later on the extension of the analysis to other polarized contributions besides the longitudinal cross section.

We now proceed as follows. First, we discuss the general properties of the angular coefficient (1) illustrating the physics potential of precision measurements of DY angular distributions at the LHC Run III and HL-LHC. Next, we focus on its application to the profiling of the gluon distribution using the open-source fit platform `xFitter` [48], and compute the resulting Higgs boson cross section and PDF uncertainty at $\sqrt{s} = 13$ TeV.

Longitudinally polarized angular coefficient. The longitudinally polarized coefficient A_0 in Eq. (1) vanishes in the parton model and receives leading-order (LO) perturbative QCD contributions at $\mathcal{O}(\alpha_s)$. We evaluate A_0 at LO and NLO (i.e., through $\mathcal{O}(\alpha_s^2)$) using the `MadGraph5_aMC@NLO` [49] program. In Fig. 1 we show results for A_0 at the energy $\sqrt{s} = 13$ TeV versus the boson transverse momentum p_T for three distinct kinematic regions: two of them at central rapidity $|Y| < 1$ with invariant mass M close to the Z boson mass M_Z as well as between the J/ψ and Υ resonances, corresponding to ATLAS and CMS kinematics; and one at $|Y| > 3.5$ and M close to M_Z, corresponding to LHCb kinematics. We also show separately the contributions to A_0 from the initial-state partonic channels $q\bar{q}$ and qg (qq and gg channels are present at NLO but they are suppressed by relative order α_s).

The coefficient A_0 as well as its $q\bar{q}$ and qg components rise monotonically from 0 at $p_T = 0$ to 1 for $p_T \gg M$. The gluonic channel qg dominates over the fermionic channel $q\bar{q}$, for the low mass region in particular. The weight of the $q\bar{q}$ contribution increases for the Z pole region and reaches its largest value for the LHCb phase space. This can be understood since the x range probed for the PDFs is changing from low to high x values. Measuring the location of A_0 with respect to the $q\bar{q}$ and qg contributions can constrain the $\bar{q}/g$ ratio, thereby giving information for the gluon and singlet quark PDFs. This confirms through NLO the features from the LO geometric picture [37, 38] of the lepton angular distributions.

The main sensitivity to the gluon distribution arises from the A_0 region where the slope in the transverse momentum, p_T, is largest, i.e., around the turn-over point $\partial^2 A_0/\partial p_T^2 = 0$. Fig. 1 illustrates that the position of this turn-over point varies strongly with a power-like dependence on the lepton-pair invariant mass, so that the mass provides a powerful handle on the transverse momentum scales probed in the initial state distribution. Near the Z-boson peak the turn-over occurs at p_T of the order of

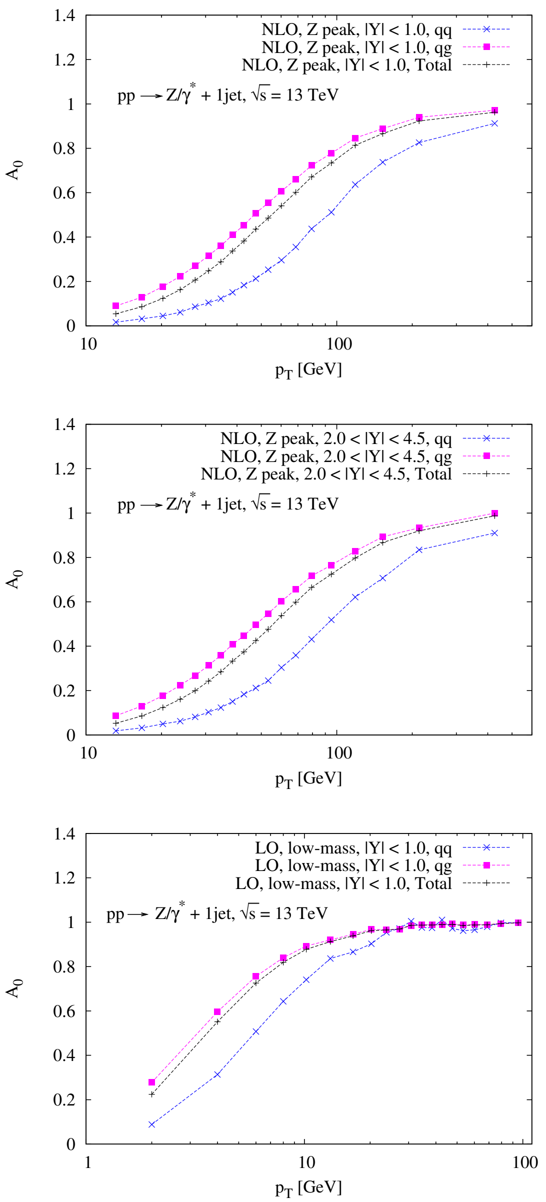

FIG. 1. The angular coefficient A_0 and its $q\bar{q}$, qg contributions for $\sqrt{s} = 13$ TeV as functions of the boson transverse momentum p_T based on CT18nnlo PDF set. The results are plotted in different regions of the boson invariant mass M and rapidity Y: the Z-boson peak region, 80 GeV $< M <$ 100 GeV, for $|Y| < 1.0$ (NLO, top); Z-boson peak region, 80 GeV $< M <$ 100 GeV for LHCb kinematics (NLO, center); low-mass region between the J/Ψ and Υ resonances, 4 GeV $< M <$ 8 GeV, for $|Y| < 1.0$ (LO, bottom).

several ten to 100 GeV, while at low masses, between the J/Ψ and Υ meson resonances, it is at p_T of the order of a few GeV. This behavior is to be contrasted with the case of the unpolarized cross section, which peaks at low p_T, with the position of the peak depending only very mildly on the invariant mass. Thus, we will use the longitudinally polarized angular distribution near the electroweak boson mass scale in order to constrain the gluon PDF in the region relevant [50] for Higgs boson production. On the other hand, the above observations suggest that the angular distribution in the low-mass range could provide sensitivity to the transverse momentum dependent gluon PDF [22, 51, 52].

New features therefore arise in the extraction of non-perturbative QCD contributions owing to the vector boson polarization. While the unpolarized spectrum is characterized by the Sudakov peak at low p_T and receives large perturbative corrections requiring all-order resummation for $p_T \ll M$, the monotonic p_T increase with M-dependent turn-over in Fig. 1 and the smallness of perturbative corrections for any p_T can be helpful in disentangling non-perturbative effects, whether of collinear or transverse momentum dependent type [53], compared to the unpolarized case. In what follows we carry out a detailed analysis for collinear distributions.

Gluon profiling and Higgs cross section. To analyze the impact of high-precision A_0 measurements on the Higgs boson production cross section, we implement the NLO `MadGraph5_aMC@NLO` A_0 calculation into the fit platform `xFitter` [48]. First, we validate our implementation by performing NLO fits to the $\sqrt{s} = 8$ TeV ATLAS measurements [41] of A_0, and verifying that good χ^2 values are obtained for all the PDF sets considered, namely CT18nnlo [5], NNPDF3.1nnlo [6], ABMP16nnlo [7], HERAPDF2.0nnlo [10] and MSHT20nnlo [11]. Next, we generate A_0 pseudodata at energy $\sqrt{s} = 13$ TeV for two projected luminosity scenarios of 300 fb^{-1} (the designed integrated luminosity at the end of the LHC Run III) and 3 ab^{-1} (the designed integrated luminosity at the end of the HL-LHC stage [14]), and apply the profiling technique [54, 55] to evaluate the PDF uncertainties. To do this we extrapolate the statistical uncertainties for the two projected integrated luminosities, and estimate the systematic uncertainties assuming a 0.1% systematic uncertainties on the lepton momentum scale. We perform the analysis in the mass region 80 GeV $< M <$ 100 GeV around the Z-boson peak and rapidity region $|Y| < 3.5$. The results are reported in Fig. 2.

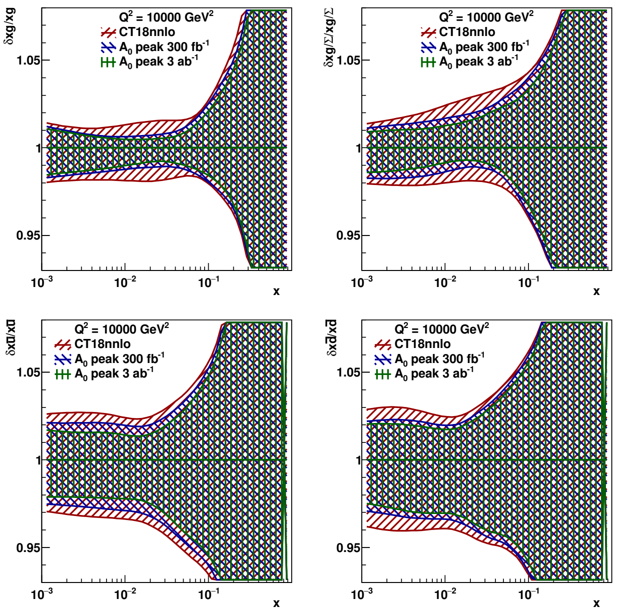

FIG. 2. Original CT18nnlo [5] (red) and profiled distributions using A_0 pseudodata corresponding to integrated luminosities of 300 fb^{-1} (blue) and 3 ab^{-1} (green) for 80 GeV $< M <$ 100 GeV and $|y| < 3.5$. Results for gluon, gluon/Sea, u-type and d-type sea-quark densities are shown for $Q^2 = 10^4$ GeV^2. Bands represent PDF uncertainties, shown at the 68% CL.

We find that, in accord with the earlier discussion, the largest reduction of uncertainties from the high-luminosity A_0 profiling occurs for the gluon density, and for the u and d sea-quark densities coupled to gluons through QCD evolution. This affects longitudinal momentum fractions x in the region $10^{-3} \lesssim x \lesssim 10^{-1}$. We also find that the largest sensitivity comes from transverse momenta in the mid range $p_T \sim 50$ GeV, and the sensitivity dies out for $p_T \gtrsim 100$ GeV. We have also verified the perturbative stability of our results, by repeating the profiling with variation of the perturbative factorization and renormalization scales in the pseudodata and finding no significant deviations.

The effect of the longitudinally polarized coefficient on the $Q^2 = 10^4$ GeV^2 gluon PDF near $x \sim 10^{-2}$ will influence the Higgs boson cross section. To study this, we compute SM Higgs boson production in the gluon fusion mode for $\sqrt{s} = 13$ TeV pp collisions, using the MCFM code [56, 57] at NLO in QCD perturbation theory. We evaluate PDF uncertainties on the Higgs cross section including constraints from A_0 profiling. The results are given in Fig. 3 versus the Higgs boson rapidity y_H. We see that in the region $-2 \lesssim y_H \lesssim 2$ the uncertainty is reduced by about 30 - 40 % in the Run III scenario, and a further reduction to about 50 % takes place in the HL-LHC scenario.

We next perform a higher-order N^{3}LO calculation for the Higgs boson total cross section using the code `ggHiggs` [58, 59]. In Fig. 4 we report the result for the cross section and its uncertainty in the cases of the current CT18nnlo [5], NNPDF3.1nnlo [6] and MSHT20nnlo [11] global sets as well as projected sets, based on complete LHC data sample [60]. Notwithstanding the numerical differences, the behavior is qualitatively similar for the different sets, and provides further

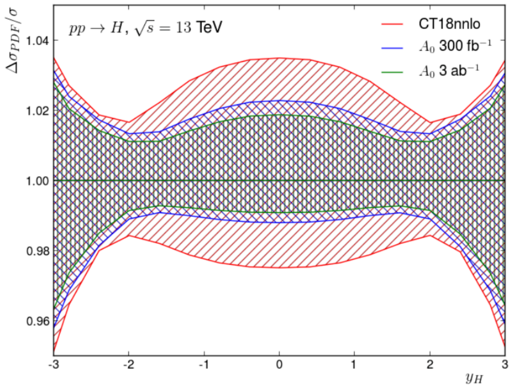

FIG. 3. Ratio of PDF uncertainties for the gluon-gluon fusion SM Higgs boson cross-section in pp collisions at $\sqrt{s}$ =13 TeV as a function of the Higgs rapidity. The red band shows the uncertainties of the CT18nnlo PDF set [5], reduced to 68% CL coverage. The blue and green bands show the uncertainties of the CT18nnlo including constraints from the A_0 measurement and assuming 300 fb^{-1} and 3 ab^{-1}, respectively.

support at N^{3}LO to the picture given in Fig. 3 for the NLO Higgs rapidity cross section.

The results above for the Higgs production cross section have been obtained using the DY angular coefficient for longitudinal electroweak boson polarization in the mass region near the Z-boson mass. We stress that the same approach, extended to mass regions away from the Z peak, has the potential to provide complementary physics information. For instance, high-mass DY angular distributions allow the region of larger x momentum fractions to be accessed and will be relevant for associated Higgs production with a gauge/Higgs boson or heavy-flavour quarks. Conversely, we have noted earlier that low-mass A_0 measurements may be used to probe transverse momentum dependent gluon PDF effects, and this will impact the Higgs boson transverse momentum spectrum for low transverse momenta. The extension to low masses can further provide a handle on the small-x regime [59, 61] of Higgs boson production relevant to the highest energy frontier. We also observe that the result in Fig. 2 for the ratio of the gluon to sea-quark densities points to possible applications in Higgs production channels other than gluon fusion, such as weak boson fusion.

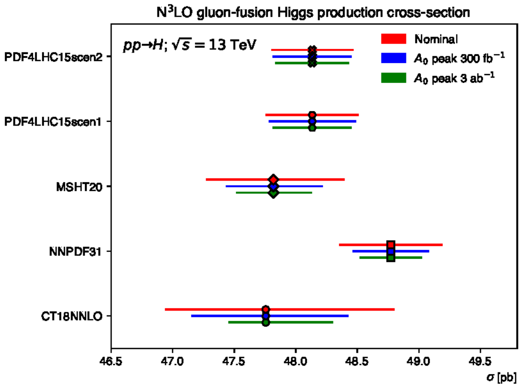

FIG. 4. The gluon-gluon fusion Higgs production cross-section at N^{3}LO for different PDFs, showing the uncertainty from PDFs and their expected reduction including constraints from the A_0 measurement assuming 300 fb^{-1} and 3 ab^{-1}, respectively.

We have so far exploited the sensitivity of the longitudinal electroweak boson polarization to the gluon PDF and singled out A_0 as a perturbatively stable observable, which can be built via diagonal elements of the polarization density matrix and is measurable via the lepton polar angle θ. This can be generalized as further sensitivity may arise from off-diagonal density matrix elements via longitudinal-transverse interferences, such as the parity-conserving A_1 and parity-violating A_3 coefficients [41], which can be accessed by measuring also the lepton azimuthal angle ϕ. These coefficients are generally smaller than A_0 and with a milder p_T dependence, but provide a more pronounced Y rapidity dependence. Moreover, starting at order α_s^2 one may investigate additional handles from violation of the Lam-Tung relation [23], $A_2 \neq A_0$, and from the T-odd coefficients A_5, A_6, A_7 [41].

Conclusion. We have proposed the systematic use of electroweak gauge boson polarization in lepton-pair hadro-production to investigate gluon-initiated processes and the associated non-perturbative QCD contributions.

We have illustrated this by studying the implications of precise measurements of the angular coefficient A_0 near the Z-boson mass scale on the theoretical predictions for the Higgs boson production cross section, exploiting the coupling of the longitudinal polarization to the gluon PDF through radiative contributions in α_s.

Our results open a new area of phenomenological studies on connections between the gauge and Higgs sectors of the SM, as further aspects may be investigated via generalization to the full structure of lepton angular distributions, including polarization interferences, and to mass regions far away from the Z-boson peak.

Acknowledgments. We thank H. Abdolmaleki, A. Armbruster, V. Bertone, S. Camarda, A. Cooper-Sarkar, D. Britzger, L. Harland-Lang, A. Huss, F. Olness and other `xFitter` developers for useful conversations and advice. The work of JF has been supported by the BMBF under contract 05H15PMCCA and the DFG through the Research Training Network 2149 “Strong and weak interactions - from hadrons to dark matter” and by STFC under the consolidated grant ST/T000988/1.

SUPPLEMENTARY MATERIAL

Fit to ATLAS 8 TeV data

To validate our theoretical framework based on the implementation of the NLO `MadGraph5_aMC@NLO` A_0 calculation into the fit platform `xFitter`, we consider the $\sqrt{s} = 8$ TeV ATLAS measurements [41] for the angular coefficient A_0, using the unregularised data in the three rapidity regions and removing the bins with $p_T < 11$ GeV.

We perform NLO fits which include the covariance matrices of the experimental and PDF uncertainties, for the cases CT18nnlo [5], NNPDF3.1nnlo [6], ABMP16nnlo [7], HERAPDF2.0nnlo [10] and MSHT20nnlo [11]. The results for the χ^2 values are reported in Tab. I for each of the PDF sets, showing a very good description of data for all sets.

PDF set	Total χ^2/d.o.f.
CT18NNLO	59/53
CT18Annlo	44/53
NNPDF31_nnlo_as_0118_hessian	60/53
ABMP16_5_nnlo	62/53
MSHT20nnlo_as118	59/53
HERAPDF20_NNLO_EIG	60/53

TABLE I. The χ^2 values per degrees of freedom from NLO fits to A_0 data [41] using `xFitter`, for different collinear PDF sets. PDF uncertainties are evaluated at the 68% CL.

Profiling in the low-mass region and forward region

Analogously to the profiling analysis of Fig. 2 in the Z-boson peak region, we perform the profiling analysis in the low mass region 4 GeV $< M <$ 8 GeV and forward rapidity region $|Y| > 3.5$. We report the results in Fig. 5.

Given that triggering in this kinematic domain is challenging we consider that only a 1% fraction of the data will be recorded, thereby reducing the effective luminosity by this factor. The largest reduction of uncertainties observed in this case for the gluon distribution is at $x < 0.001$. For the LHCb phase space, the most relevant improvements are for the sea quark PDFs, e.g. $\bar{d}$ at $x \sim 0.001$.

Gluon-gluon luminosity

We compute the gluon-gluon luminosity as a function of invariant mass to assess the reduction of uncertainties as a result of PDF profiling based on the longitudinally polarized angular coefficient A_0.

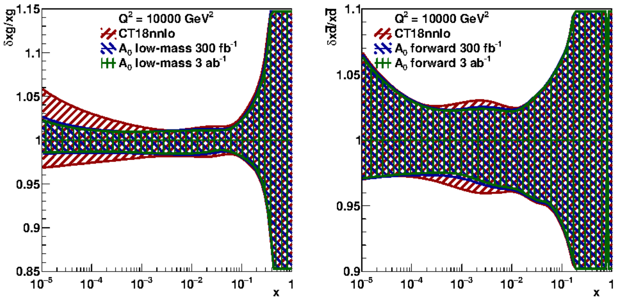

FIG. 5. Original CT18nnlo [5] (red) and profiled distributions using A_0 pseudodata corresponding to integrated luminosities of 300 fb^{-1} (blue) and 3 ab^{-1} (green) for the low mass (left) and LHCb phase space (right). Results for gluon, gluon/Sea, u-type and d-type sea-quark densities are shown for $Q^2 = 10^4$ GeV^2. Bands represent PDF uncertainties, shown at the 68% CL.

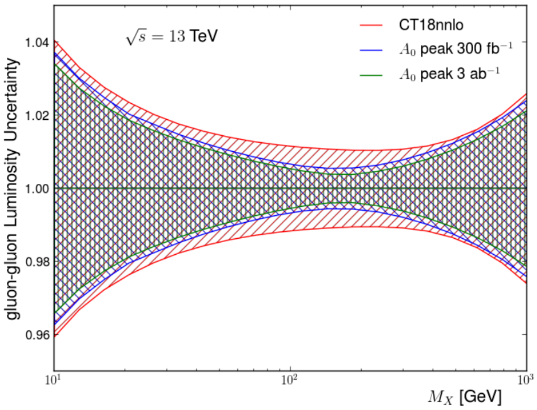

FIG. 6. Ratio of PDF uncertainties for the gluon-gluon luminosity evaluated at $\sqrt{s}$ =13 TeV. The red band shows the uncertainties of the CT18nnlo PDF set [5], reduced to 68% CL coverage. The blue and green bands show the uncertainties of the CT18nnlo including constraints from the A_0 measurement and assuming 300 fb^{-1} and 3 ab^{-1}, respectively.

In Fig. 6 we show the PDF uncertainties in the gluon-gluon luminosity evaluated at $\sqrt{s}$ =13 TeV and computed with CT18nnlo, as well as including constraints from A_0 profiling. PDF uncertainties are halved in the range $100 < M_X < 200$ GeV in the HL-LHC scenario.

---

[*] simone.amoroso@desy.de
[†] fiaschi@uni-muenster.de
[‡] francesco.giuli@roma2.infn.it
[§] alexander.glazov@desy.de
[¶] hautmann@thphys.ox.ac.uk
[**] oleksandr.zenaiev@cern.ch

[1] D. de Florian *et al.* [LHC Higgs Cross Section Working Group], arXiv:1610.07922 [hep-ph].

[2] M. Cepeda *et al.*, CERN Yellow Rep. Monogr. **7** (2019) 221 [arXiv:1902.00134 [hep-ph]].

[3] F. Dulat, B. Mistlberger and A. Pelloni, Phys. Rev. D **99** (2019) 034004 [arXiv:1810.09462 [hep-ph]].

[4] C. Anastasiou *et al.*, JHEP **05** (2016) 058 [arXiv:1602.00695 [hep-ph]].

[5] T. J. Hou *et al.*, arXiv:1912.10053 [hep-ph].

[6] R. D. Ball *et al.* [NNPDF Collaboration], Eur. Phys. J. C **77** (2017) 663 [arXiv:1706.00428 [hep-ph]].

[7] S. Alekhin *et al.*, Phys. Rev. D **96** (2017) 014011 [arXiv:1701.05838 [hep-ph]].

[8] L. Harland-Lang *et al.*, Eur. Phys. J. C **75** (2015) 204 [arXiv:1412.3989 [hep-ph]].

[9] R. D. Ball *et al.* [NNPDF Collaboration], JHEP **1504** (2015) 040 [arXiv:1410.8849 [hep-ph]].

[10] H. Abramowicz *et al.* [H1 and ZEUS], Eur. Phys. J. C **75** (2015) 580 [arXiv:1506.06042 [hep-ex]].

[11] S. Bailey *et al.*, [arXiv:2012.04684 [hep-ph]].

[12] P. Agostini *et al.* [LHeC and FCC-he Study Group], [arXiv:2007.14491 [hep-ex]].

[13] C. Aidala *et al.*, arXiv:2002.12333 [hep-ph].

[14] P. Azzi *et al.*, CERN Yellow Rep. Monogr. **7** (2019) 1 [arXiv:1902.04070 [hep-ph]].

[15] O. Zenaiev *et al.* [PROSA], JHEP **04** (2020) 118 [arXiv:1911.13164 [hep-ph]].

[16] M. Cacciari, M. L. Mangano and P. Nason, Eur. Phys. J. C **75** (2015) 610 [arXiv:1507.06197 [hep-ph]].

[17] C. A. Flett *et al.*, Phys. Rev. D **101** (2020) 094011 [arXiv:1908.08398 [hep-ph]].

[18] R. Abdul-Khalek *et al.*, Eur. Phys. J. C **80** (2020) 797 [arXiv:hep-ph/2005.11327 [hep-ph]].

[19] M. Czakon *et al.*, JHEP **04** (2017) 044 [arXiv:1611.08609 [hep-ph]].

[20] S. Drell and T.-M. Yan, Phys. Rev. Lett. **25** (1970) 316.

[21] J. C. Collins and D. E. Soper, Phys. Rev. D **16** (1977) 2219.

[22] R. Angeles-Martinez *et al.*, Acta Phys. Polon. B **46** (2015) 2501 [arXiv:1507.05267 [hep-ph]].

[23] C. S. Lam and W. K. Tung, Phys. Rev. D **18** (1978) 2447.

[24] M. Chaichian, M. Hayashi and K. Yamagishi, Phys. Rev. D **25** (1982) 130 [erratum: Phys. Rev. D **26** (1982) 2534].

[25] K. Hagiwara, K. Hikasa and N. Kai, Phys. Rev. Lett. **52** (1984) 1076.

[26] E. Accomando *et al.*, JHEP **1910** (2019) 176 [arXiv:1907.07727 [hep-ph]].

[27] H. Abdolmaleki *et al.*, [arXiv:1907.08301 [hep-ph]].

[28] E. Accomando *et al.*, Eur. Phys. J. C **78** (2018) 663 [arXiv:1805.09239 [hep-ph]].

[29] E. Accomando *et al.*, Phys. Rev. D **98** (2018) 013003 [arXiv:1712.06318 [hep-ph]].

[30] J. Fiaschi *et al.*, PoS DIS **2019** (2019) 012 [arXiv:1906.11793 [hep-ph]].

[31] E. Accomando *et al.*, Phys. Lett. B **803** (2020) 135293 [arXiv:1910.13759 [hep-ph]].

[32] J. Fiaschi *et al.*, arXiv:1805.00842 [hep-ph].

[33] E. Mirkes, Nucl. Phys. B **387** (1992) 3.

[34] E. Mirkes and J. Ohnemus, Phys. Rev. D **50** (1994) 5692 [arXiv:hep-ph/9406381 [hep-ph]].

[35] E. Mirkes and J. Ohnemus, Phys. Rev. D **51** (1995) 4891 [arXiv:hep-ph/9412289 [hep-ph]].

[36] M. Lambertsen and W. Vogelsang, Phys. Rev. D **93** (2016) 114013 [arXiv:1605.02625 [hep-ph]].

[37] J. C. Peng *et al.*, Phys. Lett. B **758** (2016) 384 [arXiv:1511.08932 [hep-ph]].

[38] W. C. Chang *et al.*, Phys. Rev. D **96** (2017) 054020 [arXiv:1708.05807 [hep-ph]].

[39] R. Gauld *et al.*, JHEP **11** (2017) 003 [arXiv:1708.00008 [hep-ph]].

[40] V. Khachatryan *et al.* [CMS], Phys. Lett. B **750** (2015) 154 [arXiv:1504.03512 [hep-ex]].

[41] G. Aad *et al.* [ATLAS], JHEP **08** (2016) 159 [arXiv:1606.00689 [hep-ex]].

[42] T. Aaltonen *et al.* [CDF], Phys. Rev. Lett. **106** (2011) 241801 [arXiv:1103.5699 [hep-ex]].

[43] S. Falciano *et al.* [NA10], Z. Phys. C **31** (1986) 513.

[44] M. Guanziroli *et al.* [NA10], Z. Phys. C **37** (1988) 545.

[45] J. S. Conway *et al.* [E615], Phys. Rev. D **39** (1989) 92.

[46] L. Y. Zhu *et al.* [NuSea], Phys. Rev. Lett. **99** (2007) 082301 [arXiv:hep-ex/0609005 [hep-ex]].

[47] L. Y. Zhu *et al.* [NuSea], Phys. Rev. Lett. **102** (2009) 182001 [arXiv:0811.4589 [nucl-ex]].

[48] S. Alekhin *et al.*, Eur. Phys. J. C **75** (2015) 304 [arXiv:1410.4412 [hep-ph]].

[49] J. Alwall *et al.*, JHEP **07** (2014) 079 [arXiv:1405.0301 [hep-ph]].

[50] P. Cipriano *et al.*, Phys. Rev. D **88** (2013) 097501 [arXiv:1308.1655 [hep-ph]].

[51] L. Motyka, M. Sadzikowski and T. Stebel, Phys. Rev. D **95** (2017) 114025 [arXiv:1609.04300 [hep-ph]].

[52] D. Boer *et al.*, SciPost Phys. **3** (2017) 040 [arXiv:1709.04935 [hep-ph]].

[53] F. Hautmann, I. Scimemi and A. Vladimirov, Phys. Lett. B **806** (2020) 135478 [arXiv:2002.12810 [hep-ph]].

[54] H. Paukkunen and P. Zurita, JHEP **1412** (2014) 100 [arXiv:1402.6623 [hep-ph]].

[55] S. Camarda *et al.*, EPJC **75** (2015) 458. [arXiv:1503.05221 [hep-ph]].

[56] J. M. Campbell and R. K. Ellis, Nucl. Phys. B Proc. Suppl. **205-206** (2010) 10 [arXiv:1007.3492 [hep-ph]].

[57] J. Campbell and T. Neumann, JHEP **12** (2019) 034 [arXiv:1909.09117 [hep-ph]].

[58] M. Bonvini *et al.*, J. Phys. G **41** (2014) 095002 [arXiv:1404.3204 [hep-ph]].

[59] M. Bonvini and S. Marzani, Phys. Rev. Lett. **120** (2018) 202003 [arXiv:1802.07758 [hep-ph]].

[60] R. Abdul-Khalek *et al.*, Eur. Phys. J. C **78** (2018) 962 [arXiv:hep-ph/1810.03639 [hep-ph]].

[61] F. Hautmann, Phys. Lett. B **535** (2002) 159 [arXiv:hep-ph/0203140 [hep-ph]].